

Biomarkers of Parkinson's disease: Striatal sub-regional structural morphometry and diffusion MRI

Ali R. Khan^{a,f,1}, Nole M. Hiebert^{b,c,1}, Andrew Vo^{c,d}, Brian T. Wang^{b,f}, Adrian M. Owen^{c,d}, Ken N. Seergobin^c, Penny A. MacDonald^{c,d,e,*,1}

^a Department of Medical Biophysics, University of Western Ontario, London, Ontario N6A5C1, Canada

^b Department of Physiology and Pharmacology, University of Western Ontario, London, Ontario N6A5C1, Canada

^c Brain and Mind Institute, University of Western Ontario, London, Ontario N6A5B7, Canada

^d Department of Psychology, University of Western Ontario, London, Ontario N6A5C2, Canada

^e Department of Clinical Neurological Sciences, University of Western Ontario, London, Ontario N6A5A5, Canada

^f Robarts Research Institute, University of Western Ontario, London, Ontario N6A 5B7, Canada

ARTICLE INFO

Keywords:

Parkinson's disease
Segmentation
Biomarker
Diffusion MRI
Morphometry
Striatum

ABSTRACT

Parkinson's disease (PD) is a progressive neurological disorder that has no reliable biomarkers. The aim of this study was to explore the potential of semi-automated sub-regional analysis of the striatum with magnetic resonance imaging (MRI) to distinguish PD patients from controls (i.e., as a *diagnostic biomarker*) and to compare PD patients at different stages of disease.

With 3 Tesla MRI, diffusion- and T1-weighted scans were obtained on two occasions in 24 PD patients and 18 age-matched, healthy controls. PD patients completed one session on and the other session off dopaminergic medication. The striatum was parcellated into seven functionally disparate sub-regions. The segmentation was guided by reciprocal connections to distinct cortical regions. Volume, surface-based morphometry, and integrity of white matter connections were calculated for each striatal sub-region.

Test-retest reliability of our volume, morphometry, and white matter integrity measures across scans was high, with correlations ranging from $r = 0.452$, $p < 0.05$ and $r = 0.985$, $p < 0.001$. Global measures of striatum such as total striatum, nucleus accumbens, caudate nuclei, and putamen were not significantly different between PD patients and controls, indicating poor sensitivity of these measures, which average across sub-regions that are functionally heterogeneous and differentially affected by PD, to act as diagnostic biomarkers. Further, these measures did not correlate significantly with disease severity, challenging their potential to serve as progression biomarkers. In contrast, a) decreased volume and b) inward surface displacement of caudal-motor striatum—the region first and most dopamine depleted in PD—distinguished PD patients from controls. Integrity of white matter cortico-striatal connections in caudal-motor and adjacent striatal sub-regions (i.e., executive and temporal striatum) was reduced for PD patients relative to controls. Finally, volume of limbic striatum, the only striatal sub-region innervated by the later-degenerating ventral tegmental area in PD, was reduced in later-stage compared to early stage PD patients a potential progression biomarker.

Segmenting striatum based on distinct cortical connectivity provided highly sensitive MRI measures for diagnosing and staging PD.

1. Introduction

Parkinson's disease (PD) is a neurodegenerative condition, affecting 1% of people aged 65 or older in industrialized countries (Goldman & Postuma, 2014), characterized by disabling motor and non-motor

symptoms. Though dopamine-replacement medications treat motor symptoms early in PD, later in disease, these therapies are less effective, whereas other symptoms are not dopamine-responsive at all (Poewe et al., 2010). There are no cures or disease-modifying therapies (Emre, 2015). The inadequate state of current therapy urgently requires

* Corresponding author at: Brain and Mind Institute, Western Interdisciplinary Research Building, Room 5160, University of Western Ontario, London, Ontario N6A 5B7, Canada.

E-mail address: penny.macdonald@lhsc.on.ca (P.A. MacDonald).

¹ Denotes equal contributions.

<https://doi.org/10.1016/j.nicl.2018.11.007>

Received 16 June 2018; Received in revised form 14 October 2018; Accepted 12 November 2018

Available online 16 November 2018

2213-1582/ © 2018 The Authors. Published by Elsevier Inc. This is an open access article under the CC BY-NC-ND license (<http://creativecommons.org/licenses/by-nc-nd/4.0/>).

correction. The development of sensitive and reliable biomarkers is critical to aid in the diagnosis of PD and to measure the efficacy of new treatments aiming to slow, halt, or reverse PD (Tuite, 2016; Miller & O'Callaghan, 2015). *Diagnostic biomarkers* that distinguish PD patients from healthy controls will improve the appropriate enrollment of patients in clinical trials. *Progression biomarkers* that objectively track disease evolution are needed to act as endpoints for critical tests of potential treatments. Prevention or delay of disease progression can only be ascertained if these objective endpoints are available. Clinical response alone is an insufficient measure that is subjective and confounds symptom-alleviating with disease-altering impacts (Strimbu & Tavel, 2010).

Magnetic resonance imaging (MRI) offers substantial promise to provide biomarkers of PD. There have been advances in determining potential structural (Rahmim et al., 2017; Sulzer et al., 2018; Sierra et al., 2017; Guan et al., 2017; Saeed et al., 2017) and functional (Saeed et al., 2017; Tang et al., 2017) biomarkers, such as differential dopamine transporter expression (Rahmim et al., 2017; Sierra et al., 2017) and mapping of iron deposition in the dopaminergic midbrain (Sulzer et al., 2018; Guan et al., 2017). Despite early promise, this literature is still in its infancy. Most of these studies fail to include a measure of test-retest reliability of the scanning protocol. Further, recent reviews of structural (Saeed et al., 2017; Mak et al., 2015; Al-Radaideh & Rababah, 2016; Yang et al., 2018; Guimaraes et al., 2018), and functional (Miller & O'Callaghan, 2015; Tahmasian et al., 2015; Weingarten et al., 2015) neuroimaging in PD reveal few consistent patterns. Most unexpectedly, structural abnormalities in the striatum, the most dopamine-depleted brain region in PD and the region that mediates the cardinal motor manifestations, are not consistent (Politis, 2014; Pyatigorskaya et al., 2014), requiring large numbers of participants (Tuite, 2016; Hopes et al., 2016; Lewis et al., 2016), though biomarkers ultimately need to be sensitive at even the single-subject level. The clinical role of neuroimaging in PD is poorly developed.

The striatum can be subdivided in a number of ways. Typically, it is divided into the nucleus accumbens, the caudate nuclei, and the putamen because these are separable at a gross level of inspection. This division, however, does not respect important differences in dopamine supply. Segmenting the striatum into its ventral (i.e., VS) and dorsal (i.e., DS) aspects separates these structures on the basis of different dopaminergic inputs. The VS, comprising the nucleus accumbens and most ventral parts of caudate nuclei and putamen, receives dopamine from the ventral tegmental area (VTA; Kish et al., 1988) whereas the DS, including the bulk of the caudate nuclei and the putamen, is supplied with dopamine from the substantia nigra pars compacta (SNc) (Kish et al., 1988). This distinction is important as the VTA degenerates later and less in PD than the SNc (Hornykiewicz, 1998; Alberico et al., 2015). Even within the SNc-innervated DS, segments of striatum are predicted to be dopamine-deprived to varying extents and at different times in PD. The cardinal motor symptoms of PD arise when the loss of dopamine-producing cells in SNc is sufficient to seriously restrict dopaminergic input to the *caudal-motor segment* of the DS (Kish et al., 1988; Fearnley & Lees, 1991; McRitchie et al., 1997). The caudal-motor segment consists of the dorsal, caudal putamen, and is the region that is presumed to be first and most dopamine depleted in PD.

In addition to these expected disparities in dopamine innervation, sub-regions of the striatum receive glutamatergic projections from distinct cortical regions that account for functional differences across these sub-regions.

Structural measurement of total striatum, nucleus accumbens, caudate nuclei, or putamen involves averaging across regions that differ in their dopamine-depletion and functions, potentially accounting for the insensitivity of structural measures of the striatum to differentiate PD patients from controls to date. Further, this might explain why estimates of total striatal volume or shape (i.e., morphology) are unreliable

across studies that include samples of PD patients who differ in PD stage, severity, and subtype. The expected evolution of dopamine denervation across regions of the striatum in PD, based on pathological studies, coupled with the increasing understanding of the functional heterogeneity across sub-regions of the striatum presents a clear biological motive to pursue sub-regional analysis of the striatum. This understanding suggests that changes in volume and shape of distinct sub-regions of the striatum could provide a) sensitive and reliable biomarkers of PD and its progression, as well as b) an explanation for symptoms that emerge at different disease stages. To our knowledge, this type of analysis has never previously been applied to PD.

1.1. Current study

A specific aim of the current study was to explore the potential of sub-regional analysis of the striatum to distinguish PD patients from controls as well as to distinguish patients at different stages of PD. We implemented an MRI segmentation proposed by Tziortzi et al. (2011; 2014). This segmentation was informed by a meta-analysis of functional MRI (fMRI) studies and guided by cortical regions to which distinct sub-regions of striatum are reciprocally connected. The proposed parcellation divides the striatum into seven sub-regions: caudal-motor, limbic, rostral-motor, executive, parietal, occipital, and temporal regions, based on reciprocally connected cortical regions (Fig. 1A).

The *caudal-motor striatum* is defined by its reciprocal connections to the primary motor and premotor cortices, comprising the caudal putamen and a small segment of anterior dorsal caudate. The caudal-motor striatal sub-region includes the segment that is presumed first and most dopamine-depleted in PD (Kish et al., 1988; Fearnley & Lees, 1991; McRitchie et al., 1997). Dopaminergic denervation of this sub-region causes motor symptoms, prompting PD diagnosis, and should therefore be affected in all PD patients, regardless of disease stage. We therefore predict that measures of caudal-motor striatum will be most sensitive to PD versus control group differences and hence will have highest diagnostic value. The *limbic striatum*, receiving cortical input from medial and ventral prefrontal regions, such as the orbitofrontal cortex, comprises the nucleus accumbens and ventral caudate and putamen, essentially constituting the VS. This limbic striatal subdivision is also very important in PD as it represents the only portion of striatum that is innervated by VTA. It is contended that VTA is relatively spared compared to SNc, especially in early PD (Kish et al., 1988; Hornykiewicz, 1998). In this way, limbic striatal measures are expected to be most differentially impacted by disease stage. We therefore expect that measures of limbic striatum have greatest potential to act as biomarkers of disease progression. Contrasting the effect of disease stage on structural measures of limbic striatum relative to other SNc-innervated portions of striatum provides a clear opportunity to test proposals regarding the pathophysiology of disease progression in PD that are widely accepted (Nyberg et al., 2015; Dean 3rd et al., 2016).

In the current study, we contrasted a sample of PD patients and healthy controls on a) global volumes of striatum, caudate nuclei, putamen, and nucleus accumbens, versus b) volume, shape, and connectivity of the seven striatal sub-regions segmented based on their cortical connectivity and function as suggested by Tziortzi et al. (2011; 2014). Within our PD sample, we further investigated whether striatal sub-regional volumes correlated with disease progression, estimated with the motor sub-scale of the Unified Parkinson's Disease Rating Scale (UPDRS-III).

A biomarker of PD must be test-retest reliable. An important additional aim of the current study was to investigate the test-retest reliability of our proposed structural measures and analysis approaches. Toward this end, structural MRIs were obtained from PD patients and controls on two occasions separated by no more than one week. In this

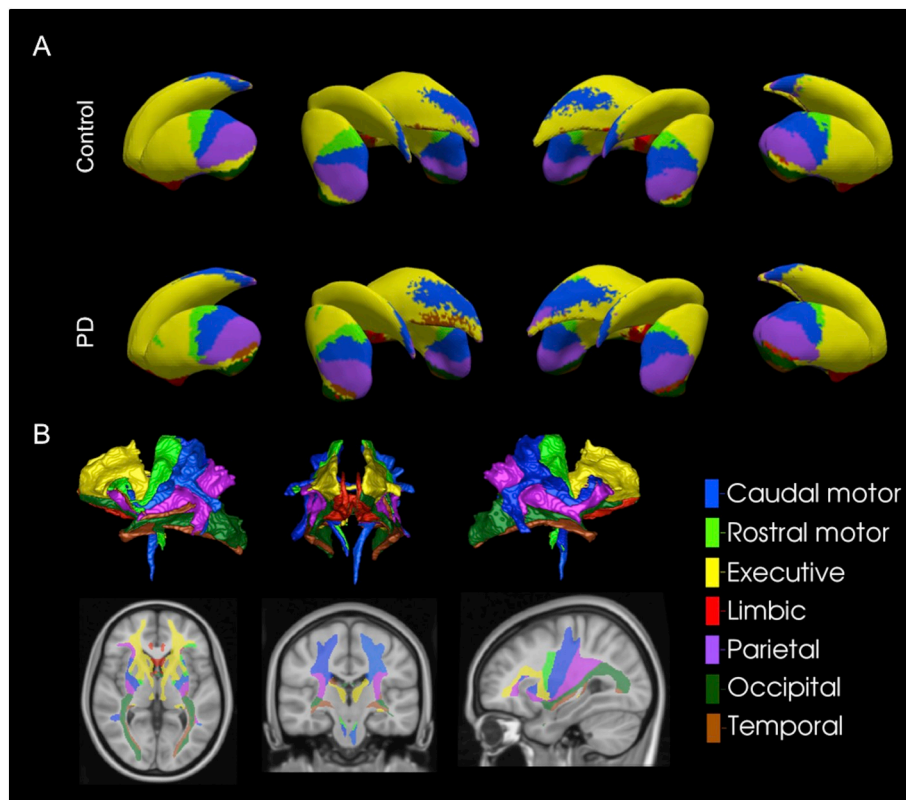


Fig. 1. Visualization of A) the connectivity-based sub-regional parcellation of the striatum for controls and PD patients, and B) the connected white matter tracts between sub-regions and the cortex (control subjects).

way, differences in our structural estimates across occasions could owe only to measurement error.

2. Methods

2.1. Participants

Twenty-four PD patients and 18 healthy, age- and education-matched controls completed the study. All participants with PD were previously diagnosed by a licensed neurologist, had no co-existing diagnosis of dementia or another neurological or psychiatric disease, save for mild depression or anxiety. All PD patients met the core assessment criteria for surgical interventional therapy and the UK Brain Bank criteria for the diagnosis of idiopathic PD (Hughes et al., 1992). All PD and no control participants were treated with dopaminergic therapy. Healthy controls were required to be within 5 years of age and of education to the PD patient to whom they were matched (see Table 1). Participants with PD were recruited through a movement disorders database at the London Health Sciences Centre. Participants abusing alcohol, prescription or illicit drugs, or taking cognitive-enhancing medications including donepezil, galantamine, rivastigmine, memantine, or methylphenidate were excluded from participating, as were patients who were diagnosed before the age of 45, had more than two first-degree relatives with PD, or had contraindication to MRI. No participants in this study were diagnosed with dementia or an impulse control disorder.

Table 1

Demographic and clinical screening measures for PD patients and controls ON and OFF medication.

Group	PD	Control	p-value
<i>n</i>	24	18	
Age	68.12 (1.10)	66.06 (2.12)	0.355
Education	15.94 (0.62)	15.76 (1.09)	0.877
Age of Onset	61.64 (1.39)		
Duration	6.48 (0.74)	–	
LED	600.32 (59.32)	–	
DA	11	–	
H & Y	2.52 (0.02)	–	
UPDRS-III	OFF 19.03 (1.00)	0.15 (0.12)	< 0.001
	ON 16.03 (1.06)	–	
BDI-II	OFF 8.09 (1.16)	2.44 (0.70)	0.001
	ON 8.33 (1.31)	2.50 (0.67)	0.001
BAI-I	OFF 7.38 (1.48)	1.72 (0.48)	0.003
	ON 8.19 (1.59)	2.61 (0.54)	0.006
ANART	123.57 (1.45)	123.90 (1.80)	0.892
MOCA	27.40 (0.32)	28.22 (0.37)	0.123

Values are reported as mean (\pm SEM). *P*-values measure the significance of the between group differences in each relevant category. LED = ν -dopa equivalence dose (mg/daily); DA = Number of individuals prescribed a dopamine agonist; H & Y = Hoehn and Yahr scale score; UPDRS-III = Unified Parkinson's Disease Rating Scale – Motor sub-scale; BDI-II = Beck Depression Inventory II; BAI-I = Beck Anxiety Inventory I; ANART = American Adult National Reading Test estimate of verbal IQ; MOCA = Montreal Cognitive Assessment. Patients with PD completed the ANART and MOCA on medication regardless of medication order.

2.2. Procedures

The UPDRS-III and Hoehn and Yahr scale was scored by a licensed neurologist with sub-specialty training in movement disorders (PAM) to assess the presence and severity of motor symptoms for all patients both on and off dopaminergic medication. Control participants were also screened with the UPDRS-III to rule out undiagnosed neurological illness. Mean group demographics, as well as cognitive and affective screening scores for all patients and controls in each experimental group were recorded (Table 1). For PD patients, duration of disease and daily doses of dopamine replacement therapy in terms of L-dopa equivalents were calculated and presented in Table 1. Calculation of daily L-dopa equivalent dose (LED) for each patient was based on the theoretical equivalence to L-dopa as follows: L-dopa dose (mg) \times 1 + L-dopa controlled release (mg) \times 0.75 + L-dopa (mg) \times 1/3 if on entacapone + amantadine (mg) \times 1 + apomorphine (mg) \times 10 + bromocriptine (mg) \times 10 + pergolide (mg) \times 100 + pramipexole as salt (mg) \times 67 + rasagiline (mg) \times 100 + ropinirole (mg) \times 20 + selegiline (mg) \times 10 (Tomlinson et al., 2010).

All participants completed two MRI sessions. PD patients performed one session on and the other off dopaminergic medication. During ON testing sessions, PD patients took their dopaminergic therapy as prescribed by their treating neurologist. During OFF testing sessions, PD patients abstained from taking all dopaminergic medications including: dopamine precursors such as L-dopa, aromatic-L-amino-acid decarboxylase inhibitors such as carbidopa, and catechol-O-methyltransferase (COMT) inhibitors such as entacapone for a minimum of 12 to a maximum of 18 h, and dopamine agonists, such as pramipexole, ropinirole or pergolide, as well as amantadine, rasagiline, and selegiline for 16 to 20 h before beginning OFF testing sessions. All patients confirmed that they complied with these instructions. UPDRS-III was performed for further confirmation. The ON-OFF order was counterbalanced across participants and though healthy controls did not take dopaminergic therapy during any session, their sessions were labelled as ON-OFF to correspond to the order of the PD patient to whom they were matched. Matching was performed at time of testing, prior to data analysis. This controlled for possible order, fatigue, and practice effects.

All participants provided informed written consent to the protocol before beginning the experiment, according to the Declaration of Helsinki (2013). All participants with PD were competent and had the capacity to provide informed consent. This study was approved by the Health Sciences Research Ethics Board of the University of Western Ontario.

2.2.1. Image analysis overview

T₁-weighted structural images as well as a DTI series were collected twice for each participant. Structural images were processed to segment the striatum, and to parcellate sub-regions based on cortical connectivity. A surface-based framework was used to measure local striatum deformations and connected white matter integrity, with all measurements taken on points that share correspondence to a common striatum surface template. Briefly, the steps taken to achieve this were to 1) segment the striatum and cortical regions using an atlas-based approach, 2) generate a canonical surface template (Fig. 2A) and fit it to each participant's striatum (Fig. 2B), and 3) employ these warped templates to perform surface-based tractography and morphometry (Fig. 2C). Maximum connectivity parcellations for each participant were calculated to generate participant-specific estimates of striatal surface area connected to each cortical region. These were then averaged across participants to generate a common parcellation map to summarize regional metrics of connected white matter integrity (i.e., fractional anisotropy; FA), and local surface morphometry for later estimating inward and outward displacement for individual participants (Fig. 2D).

2.2.2. Structural MRI acquisition

ON and OFF scanning sessions were identical. MRI scanning took place at the Roberts Research Institute at the University of Western Ontario on a Siemens Prisma Fit 3T scanner. A scout image for positioning the participant was first obtained. This was followed by a magnetization-prepared rapid acquisition with gradient echo (MPRAGE) sagittal T₁-weighted scan with the following parameters; repetition time (TR) = 2300 ms; echo time (TE) = 2.98 ms; flip angle = 9°; matrix size = 256 \times 256 pixels; and with one whole brain image consisted of 192, 1 mm-thick slices. The field of view was oriented along the anterior and posterior commissure with a matrix of 256 \times 256 pixels, an isotropic voxel size of 1 \times 1 \times 1 mm³. A diffusion-weighted echo-planar imaging (DWI) series (gradient directions = 64, b-value = 1000 s/mm², isometric voxel size of 2 mm, matrix size of 128 \times 128 pixels) was also acquired in each session in PD patients and controls.

2.2.3. T₁ and DWI pre-processing

Structural and diffusion images were first imported into NIFTI volumes using dcm2nii. Pre-processing of the T₁-weighted image included skull-stripping (FSL BET), non-uniformity correction (N4), and intensity normalization. The DWI pre-processing included linear registration to the b₀ image (FSL eddy correct), skull-stripping (FSL BET), co-registration to the T₁-weighted image (NiftyReg), tensor fitting (FSL dtfit), and fibre modelling for probabilistic ball and stick tractography (FSL BEDPOST). Processing was carried out using in-house and openly available image processing scripts (<https://github.com/khanlab/diffparc-sumo>). Quality assurance was verified at each stage of the pipelines using generated overlay images, with registration failures corrected using alternative initialization parameters.

2.2.4. Atlas-based segmentation

Structural striatum labels (caudate, putamen, VS, and a probabilistic labelling of the entire striatum) were obtained from the MNI152 1 mm atlas supplied with FSL (<http://fsl.fmrib.ox.ac.uk/fsl/fslwiki/Atlases/striatumstruc>), and cortical target regions were adapted from the Harvard-Oxford FSL atlas. The cortical target region labelling on the MNI152 1 mm atlas was based on the Tziortzi et al. (2011; 2014) striatal connectivity atlas, and consisted of caudal-motor, limbic, rostral-motor, executive, parietal, occipital, and temporal regions, as described earlier. Atlas-based segmentation of each participant was performed using the NiftyReg linear and deformable b-spline registration tools (Modat et al., 2014; Modat et al., 2010). Volumes of the striatum sub-region labels, caudate, putamen, VS were extracted from the automated segmentations. Once again, quality assurance for each registration was performed, and failures in linear registration were corrected by initialization with an alternate subject transformation matrix.

2.2.5. Canonical surface template generation and fitting

The probabilistic labels of the entire striatum in each participant were transformed back to the MNI space using obtained linear transformations, and these images, linearly aligned in the MNI space, were used to generate an unbiased average for surface generation. The large deformation diffeomorphic metric mapping (LDDMM) registration algorithm was used to generate the average, by alternating steps of template generation through averaging, and registration of each segmentation image to this template. The resulting probabilistic segmentation was then used to generate our striatum template surface through an isosurface at 50% probability. To provide point-wise correspondence between all striatum surfaces, the 3D volume of the template striatum was then fit to each participant's striatum segmentation using LDDMM, with affine initialization. The template surface was then propagated to each participant striatum, as well as the striatum in native DWI space, to provide surfaces with common indices for performing morphometry

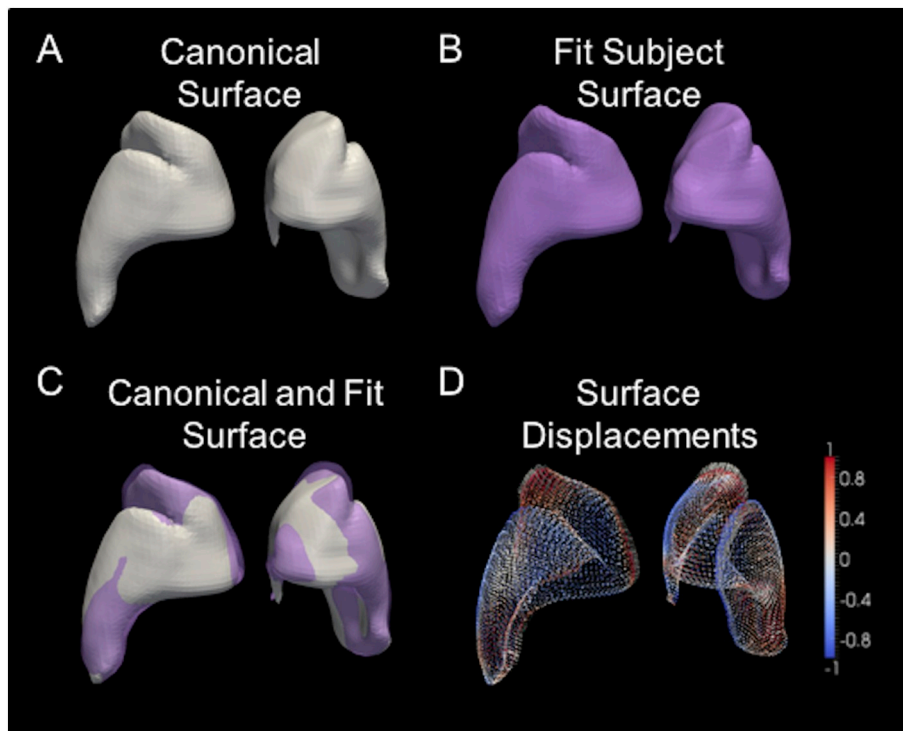


Fig. 2. Depiction of surface-based morphometry procedure for a single subject, showing the A) canonical surface, generated from an average of all subjects, B) the canonical surface warped to fit the subject anatomy, C) these two surfaces shown overlaid to highlight differences, and D) quantification of differences between these surfaces using inward (cool colours) and outward (warm colours) displacement vectors. (For interpretation of the references to color in this figure legend, the reader is referred to the web version of this article.)

and tractography. For surface morphometry, displacements at each point were computed between the template surface and the injected participant surface, using the projection along the surface normal to quantify a scalar inward/outward distance. To account for any local misalignment between the template and participant striatum surfaces, the mean displacement across a spherical neighbourhood (10 mm radius) was computed for each point and subtracted from the local point-wise displacement.

2.2.6. Tractography

Probabilistic multi-fibre tractography was performed using FSL BEDPOST (Behrens et al., 2003; Behrens et al., 2007) with the surface vertices of the striatum used as seed points. Surface meshes in VTK file format were converted to GIFTI for input into FSL BEDPOST, and 5000 seeds were initiated from each surface point. The paths taken from each point were retained and used to generate connected white-matter probability maps for sampling the FA of white matter connected to each point. Subject-specific connectivity parcellations of the striatum were created by assigning a numerical label to each surface point, based on the cortical target, out of seven possible targets, with maximal connection probability lateralized based on left and right striatum in the template, to provide a labelling of 14 regions. Tractography was also performed from all striatum segmentation voxels, to generate subject-specific volumetric parcellations, and these were linearly transformed to the MNI space for statistical analysis.

2.2.7. Regional surface-based morphometry and white matter integrity

To ensure homologous striatal surface points are used when summarizing morphometry and white matter integrity measurements, we generated a group-average parcellation based on all control participants in the study. This was done by majority voting. That is, we assign the label at each point that is shared by the greatest number of control participants. Surface-based inward/outward displacement measurements were averaged across each of the 14 regions to quantify surface morphometry. Similarly, the FA measurements were also averaged across each connected white matter region to quantify white matter integrity.

2.2.8. Output for statistical analysis

Group differences of normalized volume, surface displacement, and FA measures for functional sub-regions of striatum were investigated. In these analyses, normalized volume constituted a z-score for individual participants' volume measures for each sub-region relative to the overall average for that sub-region based on all participants in the study. This number was then multiplied by the total number of voxels contained within the striatum to yield the number of voxels in each striatal sub-region. Surface displacement and FA were calculated as described above and normalized relative to a group-average parcellation based on all control participants.

2.2.9. Statistical analyses

PD patients were compared to healthy, age- and education-matched controls. In subsequent analyses, PD patients were investigated for the effect of disease stage on structural measures. In both the ON and OFF sessions, we obtained and compared measures for PD and control participants of a) total striatum, nucleus accumbens, caudate nucleus, and putamen versus b) striatum segmented based on function into caudal-motor, limbic, rostral-motor, executive, parietal, occipital, and temporal striatal sub-regions as described above, according to the method proposed by Tziortzi et al. (2011; 2014). For all analyses, bilateral structural measures were combined and averaged to provide a single estimate of region or sub-region, in each session. For all statistical analyses, $p < 0.05$, corrected for multiple comparisons using Bonferroni correction was used as our statistical threshold. Briefly, the corrected p value was obtained by dividing the critical p value by seven (i.e. the number of striatal sub-regions under investigation).

First, the test-retest reliability of all measures was investigated with correlations between estimates obtained in the ON and OFF sessions separately for PD patients and controls.

Next, total striatum volumes as well as volumes for each the nucleus accumbens, caudate nuclei, and putamen were contrasted between PD patients and healthy controls in independent sample *t*-tests.

Independent sample *t*-tests were performed on measures of volume, surface displacement, and FA for each functional striatal sub-region, comparing PD patients to healthy controls.

Bayesian independent sample *t*-tests were conducted on all above contrasts to investigate the strength of the frequentist results. BF_{10} values of less than three, commonly indicated to be the Bayesian corollary of $p < 0.05$ in frequentist hypothesis testing, indicates that the results strongly support the null hypothesis. BF_{10} values greater than three indicate that the results strongly support the alternative hypothesis. Bayesian analyses are reported along with frequentist statistics.

Finally, within our PD group, we investigated the sensitivity of sub-regional volume measures to disease stage. The dependent measures were sub-regional volume and disease stage was estimated with UPDRS-III in the OFF state.

3. Results

3.1. Demographic and clinical contrasts

There were no significant demographic or cognitive differences between PD and control participants (Table 1). Participants with PD scored significantly higher on both BDI II and BAI compared to controls. No differences were found in terms of depressive or anxious symptoms for PD patients or controls contrasting the ON and OFF sessions. UPDRS-III scores were significantly higher in participants with PD measured off relative to on dopaminergic medication, as expected. UPDRS-III scores ranged from 10 to 25.5 for PD patients, with a mean (\pm standard error of the mean; SEM) of 19.03 (\pm 1.00) off medication and 16.03 (\pm 1.06) on medication, indicating a relatively broad range of disease. PD patients varied in disease duration from 1 to 14 years since diagnosis, with a mean (\pm SEM) of 6.48 (\pm 0.74) years. MoCA scores ranged between 22 and 30, with mean (\pm SEM) of 27.74 (\pm 0.26).

Table 2

Striatal sub-region estimates, correlations, and significance values for OFF and ON medication for PD patients and controls.

Volume	PD (n = 24)				Control (n = 18)			
	OFF	ON	r	p	OFF	ON	r	p
Total	19,296.4 (469.3)	18,974.1 (410.9)	0.819	***	18,412.0 (480.1)	18,418.7 (465.8)	0.985	***
Accumbens	2335.2 (99.9)	2347.2 (50.5)	0.652	**	2237.9 (73.4)	2217.6 (67.9)	0.944	***
Putamen	9346.8 (305.1)	9217.6 (212.7)	0.688	***	8840.0 (181.1)	8891.7 (192.5)	0.981	***
Caudate	7124.0 (254.5)	7146.8 (238.7)	0.521	*	7007.5 (264.5)	7002 (254.4)	0.984	***
Caudal-motor	1546.2 (88.4)	1628.9 (99.4)	0.621	**	1866.5 (110.5)	1772.8 (121.2)	0.575	*
Rostral-motor	1081.7 (118.1)	986.0 (108.5)	0.835	***	1008.3 (120.7)	1139.7 (150.6)	0.929	***
Executive	15,311.1 (551.8)	14,836.8 (455.5)	0.847	***	13,976.2 (784.0)	14,109.6 (776.0)	0.961	***
Limbic	1570.4 (151.9)	1659.7 (140.5)	0.610	**	1504.4 (259.8)	1416.8 (239.4)	0.948	***
Parietal	2041.6 (160.7)	2023.5 (121.8)	0.601	**	2294.4 (126.9)	2223.0 (119.7)	0.662	**
Occipital	615.7 (54.3)	532.6 (60.1)	0.700	***	589.1 (78.5)	593.3 (76.9)	0.893	***
Temporal	604.9 (128.1)	575.3 (93.1)	0.452	*	664.5 (148.0)	700.5 (114.4)	0.598	**
Displacement	PD				Control			
	OFF	ON	r	p	OFF	ON	r	p
Caudal-motor	-0.654 (0.178)	-0.679 (0.179)	0.985	***	-0.296 (0.74)	-0.324 (0.069)	0.727	***
Rostral-motor	-0.691 (0.124)	-0.660 (0.122)	0.831	***	-0.399 (0.088)	-0.427 (0.085)	0.800	***
Executive	-0.077 (0.058)	-0.089 (0.057)	0.964	***	0.0488 (0.032)	0.037 (0.037)	0.948	***
Limbic	0.758 (0.114)	0.816 (0.117)	0.891	***	0.746 (0.142)	0.759 (0.144)	0.893	***
Parietal	-0.035 (0.058)	-0.060 (0.069)	0.922	***	0.009 (0.036)	-0.001 (0.030)	0.767	***
Occipital	0.416 (0.071)	0.401 (0.066)	0.812	***	0.374 (0.069)	0.357 (0.068)	0.891	***
Temporal	0.193 (0.131)	0.146 (0.136)	0.936	***	0.322 (0.109)	0.307 (0.114)	0.980	***
Fractional Anisotropy	PD				Control			
	OFF	ON	r	p	OFF	ON	r	p
Caudal-motor	0.327 (0.009)	0.326 (0.008)	0.840	***	0.348 (0.008)	0.352 (0.009)	0.863	***
Rostral-motor	0.426 (0.006)	0.430 (0.006)	0.741	***	0.420 (0.007)	0.423 (0.007)	0.921	***
Executive	0.332 (0.004)	0.323 (0.005)	0.881	***	0.339 (0.004)	0.340 (0.005)	0.827	***
Limbic	0.335 (0.007)	0.327 (0.007)	0.645	**	0.339 (0.007)	0.341 (0.008)	0.900	***
Parietal	0.391 (0.004)	0.393 (0.004)	0.653	**	0.390 (0.008)	0.385 (0.010)	0.924	***
Occipital	0.437 (0.005)	0.440 (0.004)	0.697	***	0.434 (0.009)	0.433 (0.009)	0.983	***
Temporal	0.344 (0.005)	0.345 (0.004)	0.470	*	0.360 (0.005)	0.361 (0.005)	0.867	***

Values are reported as mean (SEM). Volume, displacement and fractional anisotropy (FA) estimates are presented for both PD patients and controls, off and on medication. Pearson correlation coefficients (*r*) between on and off sessions are presented, along with the corresponding significance (*p*) value, corrected for multiple comparisons using Bonferroni correction. ****p* < 0.001, ***p* < 0.01, **p* < 0.05.

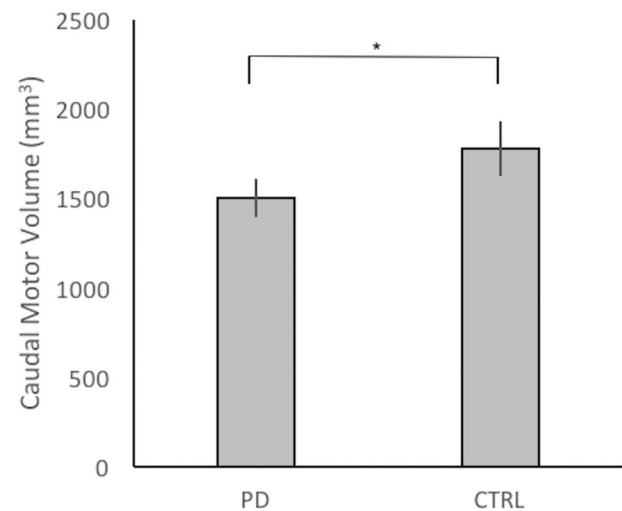


Fig. 3. Mean normalized volume of caudal-motor sub-region in mm³ for PD patients and controls. Caudal-motor volume in PD patients was significantly reduced compared to controls. * $p_{Bonferroni} < 0.05$.

3.2. Test-retest reliability

Correlations of volume estimates for total striatum, nucleus accumbens, putamen, and caudate nuclei for OFF and ON sessions were highly significant. Similarly, volume, surface displacement, and FA measures for caudal-motor, limbic, rostral-motor, executive, parietal, occipital, and temporal striatal sub-regions for OFF and ON sessions were highly significant (all $p_{Bonferroni} < 0.01$). The estimates,

correlations, and associated *p* values contrasting OFF and ON Sessions separately for PD patients and healthy controls are presented in Table 2, demonstrating high test-retest reliability for all of our measures. Given this high convergence between OFF and ON sessions, for the analyses that follow, between-session average estimates were employed.

3.3. Total striatal, nucleus accumbens, caudate nucleus, and putamen volumes

We observed no Group differences in comparing volume estimates of total striatum ($t \approx 0$, $p_{\text{Bonferroni}} \approx 0.999$, $\text{BF}_{10} = 0.441$), nucleus accumbens ($t \approx 0$, $p_{\text{Bonferroni}} \approx 0.999$, $\text{BF}_{10} = 0.366$), caudate nuclei ($t \approx 0$, $p_{\text{Bonferroni}} \approx 0.999$, $\text{BF}_{10} = 0.249$), and putamen ($t = 0.025$, $p_{\text{Bonferroni}} = 0.980$, $\text{BF}_{10} = 0.605$).

3.4. Sub-regional striatal volume measures: PD vs. control

Between group *t*-tests were performed on normalized volume for each of the seven sub-striatal regions. For the caudal-motor striatal sub-region, the difference was significant ($t = 2.24$, $p_{\text{Bonferroni}} = 0.029$, $\text{BF}_{10} = 21.965$) reflecting atrophy for PD patients relative to controls (Fig. 3).

3.5. Sub-regional displacement measures: PD vs. control

Between group *t*-tests were performed on surface displacement measures for each of the seven sub-striatal regions. The executive striatal sub-region was significantly inwardly displaced compared to controls ($t = 2.20$, $p_{\text{Bonferroni}} = 0.031$, $\text{BF}_{10} = 8.481$). The caudal-motor and rostral-motor sub-regions were both trending toward being significantly inwardly displaced compared to controls ($t = 1.98$, $p_{\text{Bonferroni}} = 0.051$, $\text{BF}_{10} = 5.626$, and $t = 1.71$, $p_{\text{Bonferroni}} = 0.092$, $\text{BF}_{10} = 3.508$ respectively). No other contrasts were significant.

3.6. FA of white matter projections to striatal sub-regions: PD vs. control

Between-group *t*-tests were performed on FA measures to each of the seven striatal sub-regions. There were significant differences between PD patients and healthy controls in the caudal-motor ($t = 2.02$, $p_{\text{Bonferroni}} = 0.047$, $\text{BF}_{10} = 6.132$), temporal ($t = 3.41$, $p_{\text{Bonferroni}} = 0.001$, $\text{BF}_{10} = 126.711$), and trending in the executive sub-region ($t = 1.92$, $p_{\text{Bonferroni}} = 0.058$, $\text{BF}_{10} = 5.167$). In all cases, the FA was decreased for PD patients relative to controls.

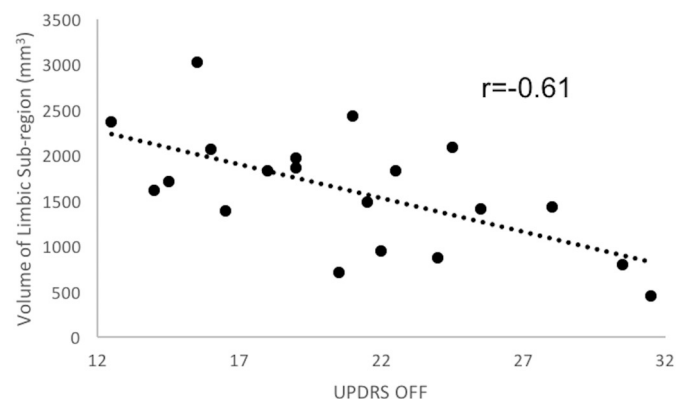


Fig. 4. Correlations between mean percentage of limbic striatum and UPDRS-III in the OFF state.

Correlation between volume of limbic striatum in mm^3 and UPDRS-III score in the OFF state. Limbic striatum volume significantly, negatively correlated with UPDRS-III score of PD patients tested in the OFF state.

3.7. Sub-regional striatal volume measures: within PD group

Within the PD group, we examined the effect of disease stage, estimated by UPDRS-III scores in the OFF state on total and sub-regional striatum volumes. The effect of disease stage was not significant on total striatum volume, $F < 1$. UPDRS in the OFF state negatively correlated with volume of the limbic striatum ($r = -0.614$, $t = 3.06$, $p_{\text{Bonferroni}} = 0.005$; Fig. 4). That is, limbic striatum volume was lower for patients with more advanced PD based on UPDRS-III scores. Correlations on volume estimates in all other striatal sub-regions were not significantly related to measures of disease stage.

4. Discussion

We segmented the striatum into seven functional regions based on reciprocal connections to cortical areas as proposed by Tziortzi et al. (2011; 2014). These consisted of caudal-motor, limbic, rostral-motor, executive, parietal, occipital, and temporal sub-regions. Estimates of volume, surface displacement relative to an average control-group template, and FA of white matter tracts between the ON and OFF medication sessions for each of the seven striatal sub-regions were highly consistent.

When total volumes of striatum, nucleus accumbens, caudate nuclei, and putamen were compared between PD patients and controls, no differences arose. In contrast, volume was reduced, surface was displaced inward, and white-matter connections were degraded for the caudal-motor striatal sub-region in PD patients compared to controls. Comparing PD patients to controls, inward surface displacement was also noted in the executive striatal sub-region, and FA, our measure of white-matter integrity, was reduced in executive and temporal striatal sub-regions. All differences were significant even after correcting for multiple comparisons. Further, all results were confirmed with Bayesian analysis.

PD patients were examined separately, exploring the effect of motor symptom severity, on striatal sub-regional volumes. The motor sub-scale of the UPDRS is an objective assessment of disease severity that accounts for significantly variable rates of disease progression across PD patients (Stebbins, 1999). UPDRS-III score significantly, negatively correlated with limbic striatum volume.

4.1. Striatal structural measures to diagnose PD

To date, there are no neuroimaging biomarkers that reliably detect the presence of PD, allowing accurate diagnosis and appropriate enrollment of patients in investigations of disease-modifying therapies (Tuite, 2016; Miller & O'Callaghan, 2015). In line with a number of previous investigations, especially when considering small samples of PD patients and healthy controls (Al-Radaideh & Rababah, 2016; Menke et al., 2014; Lee et al., 2014), there were no significant between-group differences in total striatum, nucleus accumbens, caudate nuclei, or putamen volumes, all $p > 0.900$. At first glance, this seems surprising given that the striatum is the central structure that is dopamine deprived in PD. Looking more closely, there is variability across sub-regions of the striatum in terms of how significantly and at what time they are dopamine depleted in PD. Segmenting the striatum on the basis of reciprocal connections to distinct cortical regions that are associated with different functions, using a method outlined by Tziortzi et al. (2011; 2014) we found significant atrophy and reduced structural connectivity in the caudal-motor sub-region for PD patients relative to healthy controls. This sub-region is notable because it is the first and most dopamine-depleted striatal region in PD, mediating onset of motor symptoms and hence signalling PD diagnosis (Kish et al., 1988). This region is expected to be affected in all PD patients irrespective of disease stage. In addition to a biochemical deficit, structural disruptions in the substrate of the striatum are expected to include intra-neuronal alpha-synuclein accumulation (i.e., Lewy bodies) and neuronal loss

(Fahn, 2003). Evidence suggests cell-to-cell Lewy body propagation through functional synapses (Calo et al., 2016). This presents a mechanism by which striatal sub-regional structural changes arise and subsequently a means by which cortical regions are affected by disease through white matter connections. FA, indexing integrity and density of white matter projections, seemed even more sensitive in distinguishing PD patients from controls, revealing impoverished white matter projections between cortex and caudal-motor, as well as between cortical regions and executive, and temporal striatal regions for PD patients relative to controls. Disruption of white matter connections potentially precedes neuronal or gray matter loss, explaining the greater sensitivity to earlier changes. These findings are further in line with the increasingly supported view that dysfunction across widespread networks occur in PD and underlie symptoms (Dang et al., 2012; Baggio et al., 2015).

4.2. Structural biomarkers indicating PD stage

Biomarkers sensitive to the stage of PD are critically needed, providing objective endpoints for evaluating potential disease-modifying therapies, yet, to this point, they are lacking (Tuite, 2016; Miller & O'Callaghan, 2015). Clinico-pathological studies suggest that dopamine-producing neurons in SNc and VTA are affected at different times in disease progression, with VTA degeneration arising at much later disease stages and to a lesser degree than SNc. Our results show that of the only striatal downstream target of VTA, the limbic striatum, encompassing the VS, was reduced in patients with more advanced PD based on greater motor signs as assessed with the UPDRS-III in the OFF state.

4.3. Conclusions

Sub-dividing the striatum into seven regions based on connectivity to distinct cortical regions and functional differences, using a semi-automatic pipeline which we have made freely-available, in PD patients and age- and education-matched healthy controls, we uncovered changes in volume, surface displacement, and white matter connectivity measures that were highly sensitive to presence of PD. These measures further were found to have high test-retest reliability—a required property of a biomarker of disease. We found, in our heterogeneous sample of PD patients compared to controls, that the caudal-motor region of the striatum was significantly atrophied, estimated by measures of both volume and shape. In contrast, global structural measures of the striatum defined on gross appearance (i.e., total striatum, nucleus accumbens, caudate nucleus, and putamen) were entirely insensitive to these group differences, suggesting that MRI structural measures have no role in PD diagnosis. These findings suggest that focussing in on the segment of striatum that is earliest and maximally dopamine deprived in PD, the caudal-motor striatal region, could provide a sensitive diagnostic biomarker of PD. Quantity and integrity of white matter connections to this sub segment of DS, as well as to adjacent sub segments (i.e., executive and temporal), appeared to be potentially even more sensitive to PD-control differences. Finally, in our PD sample, reduction in volume of limbic striatum, the only striatal region that is innervated by dopamine-producing neurons of the later-degenerating VTA, negatively correlated with UPDRS-III score in the OFF state, an objective measure of PD severity. In this way, we suggest a role for MRI in PD management.

Future research should aim to explore the methods proposed in this manuscript in a larger sample of PD patients who are selected and stratified to represent different PD clinical subtypes, symptoms, and disease stages. Alternations in different striatal sub-regions could yield important neuroimaging indicators of PD as well as account for the emergence of different symptoms across PD patients and disease evolution.

Funding

This work was supported by a Natural Sciences and Engineering Research Council of Canada grant (NSERC; Grant: RA4981A01), a Lawson Internal Research Fund Award (Lawson IRF), and a Canada Research Chair Tier 2 (CRC; Grant: 950-230372) to Dr. Penny A. MacDonald as well as a Canada Excellence Research Chair (CERC; Grant: 215063) award to Dr. Adrian M. Owen.

References

- Alberico, S.L., Cassell, M.D., Narayanan, N.S., 2015. The vulnerable ventral tegmental area in Parkinson's disease. *Basal Ganglia* 5 (2–3), 51–55.
- Al-Radaideh, A.M., Rababah, E.M., 2016. The role of magnetic resonance imaging in the diagnosis of Parkinson's disease: a review. *Clin. Imaging* 40 (5), 987–996.
- Baggio, H.C., Segura, B., Junque, C., 2015. Resting-state functional brain networks in Parkinson's disease. *CNS Neurosci. Ther.* 21 (10), 793–801.
- Behrens, T., Rohr, K., Stiehl, H.S., 2003. Robust segmentation of tubular structures in 3-D medical images by parametric object detection and tracking. *IEEE Trans. Syst. Man. Cybern. B Cybern.* 33 (4), 554–561.
- Behrens, T.E., Berg, H.J., Jbabdi, S., Rushworth, M.F., Woolrich, M.W., 2007. Probabilistic diffusion tractography with multiple fibre orientations: what can we gain? *NeuroImage* 34 (1), 144–155.
- Calo, L., Wegrzynowicz, M., Santivanez-Perez, J., Grazia Spillantini, M., 2016. Synaptic failure and alpha-synuclein. *Mov. Disord.* 31 (2), 169–177.
- Dang, L.C., O'Neil, J.P., Jagust, W.J., 2012. Dopamine supports coupling of attention-related networks. *J. Neurosci.* 32 (28), 9582–9587.
- Dean 3rd, D.C., Sojkova, J., Hurley, S., et al., 2016. Alterations of myelin content in Parkinson's disease: a cross-sectional neuroimaging study. *PLoS One* 11 (10), e0163774.
- Emre, M., 2015. *Cognitive Impairment and Dementia in Parkinson's Disease*. (Second edition. ed 2015).
- Fahn, S., 2003. Description of Parkinson's disease as a clinical syndrome. *Ann. N. Y. Acad. Sci.* 991, 1–14.
- Fearnley, J.M., Lees, A.J., 1991. Ageing and Parkinson's disease: substantia nigra regional selectivity. *Brain* 114, 2283–2301 Pt 5.
- Goldman, J.G., Postuma, R., 2014. Premotor and nonmotor features of Parkinson's disease. *Curr. Opin. Neurol.* 27 (4), 434–441.
- Guan, X., Xuan, M., Gu, Q., et al., 2017. Regionally progressive accumulation of iron in Parkinson's disease as measured by quantitative susceptibility mapping. *NMR Biomed.* 30 (4).
- Guimaraes, R.P., Campos, B.M., de Rezende, T.J., et al., 2018. Is diffusion tensor imaging a good biomarker for early Parkinson's disease? *Front. Neurol.* 9, 626.
- Hopes, L., Grolez, G., Moreau, C., et al., 2016. Magnetic resonance imaging features of the nigrostriatal system: biomarkers of Parkinson's disease stages? *PLoS One* 11 (4), e0147947.
- Hornykiewicz, O.O., 1998. Biochemical aspects of Parkinson's disease. *Neurology* 51 (2 suppl 2), S2–S9.
- Hughes, A.J., Daniel, S.E., Kilford, L., Lees, A.J., 1992. Accuracy of clinical diagnosis of idiopathic Parkinson's disease: a clinico-pathological study of 100 cases. *J. Neurol. Neurosurg. Psychiatry* 55 (3), 181–184.
- Kish, S.J., Shannak, K., Hornykiewicz, O., 1988. Uneven pattern of dopamine loss in the striatum of patients with idiopathic Parkinson's disease. Pathophysiologic and clinical implications. *N. Engl. J. Med.* 318 (14), 876–880.
- Lee, H.M., Kwon, K.Y., Kim, M.J., et al., 2014. Subcortical grey matter changes in untreated, early stage Parkinson's disease without dementia. *Parkinsonism Relat. Disord.* 20 (6), 622–626.
- Lewis, M.M., Du, G., Lee, E.Y., et al., 2016. The pattern of gray matter atrophy in Parkinson's disease differs in cortical and subcortical regions. *J. Neurol.* 263 (1), 68–75.
- Mak, E., Su, L., Williams, G.B., O'Brien, J.T., 2015. Neuroimaging correlates of cognitive impairment and dementia in Parkinson's disease. *Parkinsonism Relat. Disord.* 21 (8), 862–870.
- McRitchie, D.A., Cartwright, H.R., Halliday, G.M., 1997. Specific A10 dopaminergic nuclei in the midbrain degenerate in Parkinson's disease. *Exp. Neurol.* 144 (1), 202–213.
- Menke, R.A., Szewczyk-Krolkowski, K., Jbabdi, S., et al., 2014. Comprehensive morphometry of subcortical grey matter structures in early-stage Parkinson's disease. *Hum. Brain Mapp.* 35 (4), 1681–1690.
- Miller, D.B., O'Callaghan, J.P., 2015. Biomarkers of Parkinson's disease: present and future. *Metabolism* 64 (3 Suppl. 1), S40–S46.
- Modat, M., Ridgway, G.R., Taylor, Z.A., et al., 2010. Fast free-form deformation using graphics processing units. *Comput. Methods Prog. Biomed.* 98 (3), 278–284.
- Modat, M., Cash, D.M., Daga, P., Winston, G.P., Duncan, J.S., Ourselin, S., 2014. Global image registration using a symmetric block-matching approach. *J. Med. Imaging* 1 (2), 024003.
- Nyberg, E.M., Tanabe, J., Honce, J.M., et al., 2015. Morphologic changes in the meso- limbic pathway in Parkinson's disease motor subtypes. *Parkinsonism Relat. Disord.* 21 (5), 536–540.
- Poewe, W., Antonini, A., Zijlmans, J.C., Burkhard, P.R., Vingerhoets, F., 2010. Levodopa in the treatment of Parkinson's disease: an old drug still going strong. *Clin. Interv. Aging* 5, 229–238.
- Politis, M., 2014. Neuroimaging in Parkinson disease: from research setting to clinical

- practice. *Nat. Rev. Neurol.* 10 (12), 708–722.
- Pyatigorskaya, N., Gallea, C., Garcia-Lorenzo, D., Vidailhet, M., Lehericy, S., 2014. A review of the use of magnetic resonance imaging in Parkinson's disease. *Ther. Adv. Neurol. Disord.* 7 (4), 206–220.
- Rahmim, A., Huang, P., Shenkov, N., et al., 2017. Improved prediction of outcome in Parkinson's disease using radiomics analysis of longitudinal DAT SPECT images. *Neuroimage Clin.* 16, 539–544.
- Saeed, U., Compagnone, J., Aviv, R.L., et al., 2017. Imaging biomarkers in Parkinson's disease and Parkinsonian syndromes: current and emerging concepts. *Transl. Neurodegener.* 6, 8.
- Sierra, M., Martínez-Rodríguez, I., Sánchez-Juan, P., et al., 2017. Prospective clinical and DaT-SPECT imaging in premotor LRRK2 G2019S-associated Parkinson disease. *Neurology* 89 (5), 439–444.
- Stebbins, G.T.G., 1999. Factor analysis of the motor section of the unified Parkinson's disease rating scale during the off-state. *Mov. Disord.* 14 (4), 585–589.
- Strimbu, K., Tavel, J.A., 2010. What are biomarkers? *Curr. Opin. HIV AIDS* 5 (6), 463–466.
- Sulzer, D., Cassidy, C., Horga, G., et al., 2018. Neuromelanin detection by magnetic resonance imaging (MRI) and its promise as a biomarker for Parkinson's disease. *NPJ Parkinsons Dis.* 4, 11.
- Tahmasian, M., Bettray, L.M., van Eimeren, T., et al., 2015. A systematic review on the applications of resting-state fMRI in Parkinson's disease: Does dopamine replacement therapy play a role? *Cortex* 73, 80–105.
- Tang, Y., Meng, L., Wan, C.M., et al., 2017. Identifying the presence of Parkinson's disease using low-frequency fluctuations in BOLD signals. *Neurosci. Lett.* 645, 1–6.
- Tomlinson, C.L., Stowe, R., Patel, S., Rick, C., Gray, R., Clarke, C.E., 2010. Systematic review of levodopa dose equivalency reporting in Parkinson's disease. *Mov. Disord.* 25 (15), 2649–2653.
- Tuite, P., 2016. Magnetic resonance imaging as a potential biomarker for Parkinson's disease. *Transl. Res.* 175, 4–16.
- Tziortzi, A.C., Searle, G.E., Tzimopoulou, S., et al., 2011. Imaging dopamine receptors in humans with [¹¹C]-(+)-PHNO: dissection of D3 signal and anatomy. *NeuroImage* 54 (1), 264–277.
- Tziortzi, A.C., Haber, S.N., Searle, G.E., et al., 2014. Connectivity-based functional analysis of dopamine release in the striatum using diffusion-weighted MRI and positron emission tomography. *Cereb. Cortex* 24 (5), 1165–1177.
- Weingarten, C.P., Sundman, M.H., Hickey, P., Chen, N.K., 2015. Neuroimaging of Parkinson's disease: expanding views. *Neurosci. Biobehav. Rev.* 59, 16–52.
- World Medical A, 2013. World medical association declaration of Helsinki: ethical principles for medical research involving human subjects. *JAMA* 310 (20), 2191–2194.
- Yang, J., Burciu, R.G., Vaillancourt, D.E., 2018. Longitudinal progression markers of Parkinson's disease: current view on structural imaging. *Curr. Neurol. Neurosci. Rep.* 18 (12), 83.